

Chapter 11

Drying of Tiny Colloidal Droplets: A Novel Synthesis Strategy for Nano-structured Micro-granules



Debasis Sen, Jitendra Bahadur, and Avik Das

Abstract Colloids are ubiquitous, and they form an interesting branch of soft-matter science owing to the nature of interactions among the constituent phases. The stability of a colloidal dispersion is governed by various intriguing competitive forces, such as electrostatic, entropic, van der Waals interactions, etc., among its dispersed phases. If continuous medium of colloidal dispersion starts disappearing, e.g. evaporation of water from aqueous colloids, the interaction among the constituent particles gets significantly altered. In fact, the phenomenon of quick evaporation of suspension droplets, known as spray drying, is widely used in several industries including food and pharmaceutical industries. Since last decade, this novel technique has re-embellished itself in nano-science and nano-technology promising ample scope for synthesis of advanced materials. Fast-evaporating tiny colloidal droplets exhibit spectacular behaviour due to sudden transition from liquid to powder state associated with evaporation-induced assembly of the nanostructures. Using such evaporative technique, various hierarchically structured micro/meso/macroporous granules can be synthesized. The quick evaporation of the solvent owing to large available surface area of the atomized droplets, makes the process one-step and energy-efficient. The morphology of the synthesized nano-structured micro-granules can be tuned from spherical to non-spherical, such as doughnut, multi-faceted doughnut, etc. The reason behind such morphological transition is primarily associated with buckling of elastic shell that forms during evaporative assembly. These granules, owing to their characteristic structure and porosity, promise for potential technological applications too. Understanding the mesoscopic structure and correlation among the constituent nanostructures in a granule is indeed crucial. In this regard, small-angle neutron/X-ray scattering and scanning electron microscopy have been found to be effective tools in probing such correlated nano-structured granules. In this chapter, the synthesis strategy of such novel nano-structured micro-granules, their mesoscopic characterization will be elaborated.

D. Sen (✉) · J. Bahadur · A. Das

Solid State Physics Division, Bhabha Atomic Research Centre, Mumbai 400085, India

e-mail: debasis@barc.gov.in

Homi Bhabha National Institute, Anushaktinagar, Mumbai 400094, India

© The Author(s), under exclusive license to Springer Nature Singapore Pte Ltd. 2022

445

A. K. Tyagi and R. S. Ningthoujam (eds.), *Handbook on Synthesis Strategies*

for Advanced Materials, Indian Institute of Metals Series,

https://doi.org/10.1007/978-981-16-1803-1_11

Keywords Evaporation-induced assembly · Colloids · Spray drying · Porous · Micro-granules · SAXS · SANS

11.1 Introduction

Granular materials are ubiquitous in our daily life. Sand is a common example of such naturally occurring material. In general, granular material is defined as a conglomeration of discrete solid particles. They behave in a significantly different way than conventional solids, liquids or gases, which has inspired many to characterize such materials as a new form of matter. Apart from various scientific interests owing to their complex flow properties, these materials play an important role in many industries, such as mining, agriculture, civil engineering, pharmaceutical manufacturing, etc. Often the granular materials that we are regularly habituated are of macroscopic length scale. Since the last couple of decades, much attention has been paid to synthesize granular materials having smaller dimension, e.g. micrometric or sub-micrometric length scale. Of course, one extreme of this field is populated by fascinating field of nanoparticles. Thus, bottom-up approach happens to be more effective compared to top-down approach to realize such micro-granules with nanoparticles as building blocks. It is easily understandable that such nano-structured micro-granules possess several inherent interesting structural features. Due to the presence of constituent nanoparticles, the granules are expected to have large available surface area. Further, the granules are inherently micro/meso porous in nature owing to the formation of the nanoparticle interstices. Such pores facilitate a percolation path for fluid transport through these granules.

Various strategies have been made to realize such nano-structured micro-granules including various low temperature chemical routes [1–4]. However, in many cases, such methods suffer from various issues including up-scalability for laboratory to commercial production, energy efficiency and total time duration of synthesis. Most of these shortcomings regarding the synthesis of such micro-granules could be overcome by following idea from an age-old industrial technique which is known as ‘spray drying’. This technique is well known, particularly in food and pharmaceutical industries, since long time. In this process, powder particles are obtained from drying of atomized droplets of liquid solution. Milk and coffee powder are common examples of spray-dried materials used in everyday life. Since the last decade, this technique has re-embellished itself in the field of nano-science and technology by producing various novel nano-structured micro-granules [5, 6]. The main principle behind this novel one-step technique is based on interlocking of colloidal particles in drying micrometric droplets through evaporation-induced assembly (EIA) owing to the dynamic interplay between several competitive forces arising due to the modification of potential landscape as solvent evaporates. At this juncture, it is worth mentioning that such assembly process is also often seen around us, as in the case of formation of ring when a drop of coffee gets dried [7] in a cup. Unlike drying

of bulk suspension, evaporation of solvent in spray drying becomes more energy-efficient owing to availability of large surface area of the atomized droplets. However, simultaneous involvement of several dynamic physicochemical parameters, such as volume fraction [8], interparticle interaction [9, 10], diffusion of the particles [11, 12] in the drying droplet, hydrodynamic effects, etc., impose a challenge to decipher the exact role of individual parameter in order to tune the granule morphology and interparticle correlation in the granules.

11.2 Synthesis of Micro-granules by Spray Drying

In a practical situation, such evaporation-induced assembly is achieved through usage of a spray dryer. ‘*Spray*’ and ‘*Drying*’, these two words together simply define the one-step facile process involving a phase separation of colloidal suspension from its solvent and interlocking of the dispersed phase through drying of sprayed liquid droplets into a hot chamber associated with air suction. Figure 11.1 depicts the schematic diagram of the different components of a typical spray dryer. A liquid stream of colloidal suspension is fed by peristaltic/syringe pump to an atomizer, which atomizes the feed solution into tiny droplets. The transformation of bulk

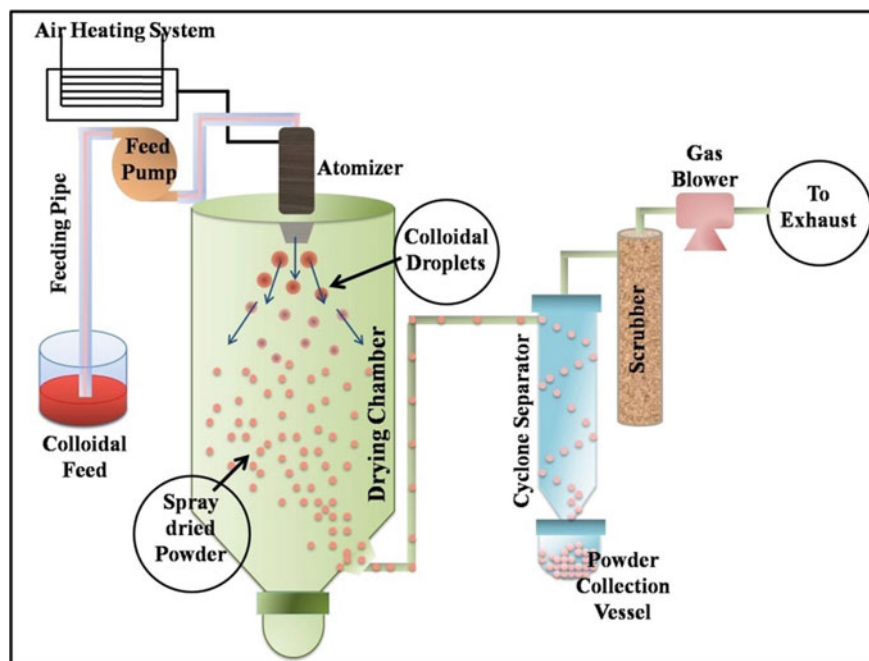


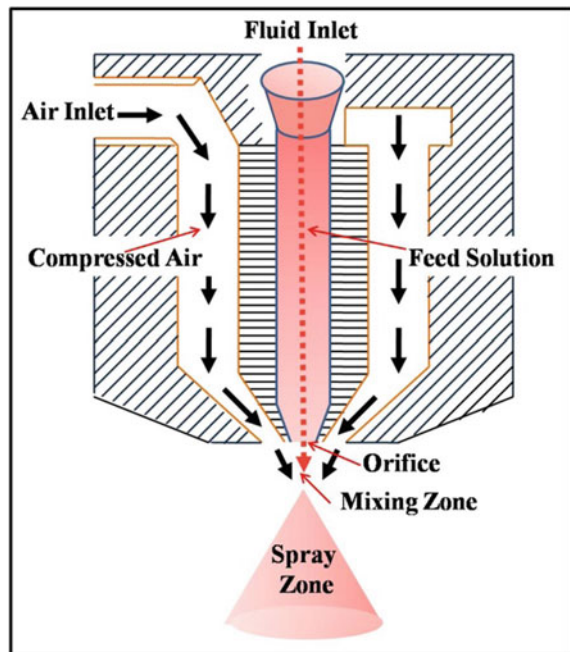
Fig. 11.1 Schematic diagram of a typical spray dryer for realizing micro-granules from colloidal dispersion

liquid into tiny droplets (typically 10–200 μm sizes) increases surface-to-volume ratio significantly, which enables more heat transfer in shorter duration of time. Controlling the atomization process, i.e. the fission of bulk liquid into large number of droplets is extremely crucial for a spray dryer as this particular process plays an important role in deciding the size distribution of the synthesized powder granules. The atomization process is familiar in everyday life which include shower heads, perfume sprays, etc. In spray drying process, normally such atomization process involves air-compressed nozzles. In air spray atomization, fluid emerging from a nozzle at low speed is surrounded by a high-speed stream of air. Friction between the liquid and air accelerates and disrupts the fluid stream and causes atomization. The energy source for air atomization is air pressure. Figure 11.2 illustrates how a stream of feed solution gets atomized while passing through an orifice. The atomized droplet size is a function of the type of atomizer nozzle and spray parameters including the feed flow rate, feed pressure, specific gravity of the feed, surface tension and viscosity of the feed [13]. However, the effective droplet size (D) can be approximated by

$$D = C P^{-n} M^l \eta^w \sigma_s^s \rho^{-t} \quad (11.1)$$

where ' P ' is the atomization pressure, ' M ' is the liquid feed rate, ' η ' is the viscosity of the liquid, ' σ_s ' is the surface tension, ' ρ ' is the density of liquid and ' C ', ' n ', ' l ', ' w ', ' s ', ' t ' being positive constants. Apart from air-compressed nebulizer, other types of atomizer also exist, such as electrostatic atomizer or ultrasonic atomizer.

Fig. 11.2 Illustrates the atomization process of fluid by compressed air at the orifice of the nozzle

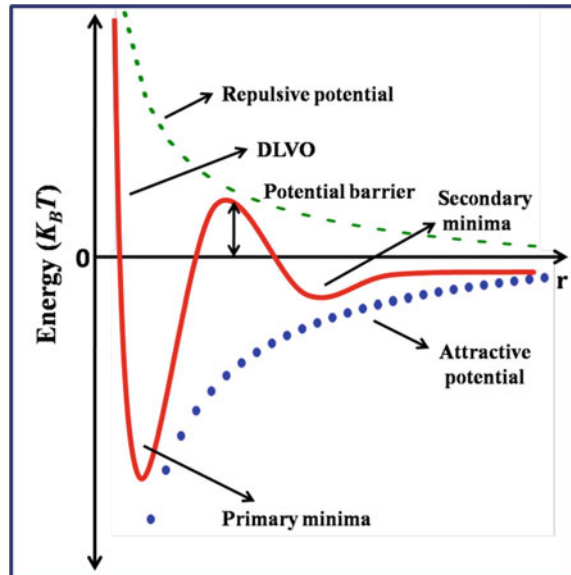


Electrostatic atomization exposes a fluid to a high electric field between the atomizer and the ground. The charge transfers to the fluid, and repulsive forces between the atomizer and the fluid tear the droplets from the atomizer. Ultrasonic atomization relies on an electromechanical device that vibrates at a very high frequency (20 kHz–10 MHz). Fluid passes over the vibrating surface, and the vibration causes the fluid to break into droplets. Ultrasonic atomizers have advantage of producing narrow size distribution of droplets as compared to polydisperse droplets produced by air-compressed atomizers. An electromechanical device made of two piezoelectric crystals that vibrate at a very high frequency governs the ultrasonic atomizer. However, ultrasonic atomization technology is primarily effective for low-viscosity Newtonian fluids. In subsequent stage of atomization, the droplets are brought into contact of hot gas in the spraying chamber. The evaporative assembly of the dispersed particles occurs in this part. The drying chamber is kept evacuated to ensure efficient evaporation and heat transfer from the hot gas to the droplets. The efficient drying at lower temperature makes the process economic. The solvent vaporizes in contact with hot gas leaving behind the micro-granules. The drying time should be less than the value of L/v , where ' L ' denotes the length of the chamber and ' v ' being the aspiration speed. The micro-granules are generally collected in cyclone separator by drawing the gas stream containing the evaporated moisture. It is worthy to mention that the rate of evaporation of the solvent molecules has a significant role to play which defines the morphology of the resultant powder and will be discussed later.

11.3 Colloidal Self-assembly During Spray Drying

It should be noted that for synthesis of the nano-structured micro-granules through spray drying, the starting ingredient is primarily a stable colloidal dispersion or sol, which is made up of dispersed phase and dispersion liquid. However, onset of evaporation during this one-step process suddenly starts altering the stability landscape owing to the continuous removal of solvent from the droplets. Thus, in order to understand the consequence of the spray drying process, it is required to discuss in brief about the stability of a colloidal dispersion where tiny dispersed particles have a typical dimension between 1 and 100 nm. The stability of a colloidal dispersion is defined by the particles remaining suspended in dispersion medium. To maintain the stability, it is required to prevent the aggregation of the colloidal particles which collide with each other through Brownian motion. For a charge stabilized system, this is generally achieved by increasing the surface charge associated with the particles. The stability of such a colloidal system is thus governed by the force balance between attractive van der Waals force and the repulsive electrostatic force. The DLVO theory (after Boris Derjaguin and Lev Landau, Evert Verwey and Theodoor Overbeek) tries to explain such stability by combining the effects of attractive and repulsive components. The typical variation of potential energy profile with interparticle distance is shown in Fig. 11.3. The combination of short-range attractive van der Waals and long-range repulsive screen Coulomb forces results in a deep attractive well, which is

Fig. 11.3 Typical DLVO potential energy profile between two colloidal particles as function of interparticle separation (r)



referred as the primary minimum. At larger distances, the colloidal particles remain stable in secondary minimum in balance with attractive and repulsive forces. When the colloids come closer to each other, repulsive force shoots up resulting in energy profile maxima, called potential barrier. This barrier prevents the aggregation of colloids in the dispersed liquid phase. However, any external force can help them to overcome the potential hill to jump into the deep attractive well vis-à-vis primary energy minimum configuration. This is where the evaporation of liquid phase of the tiny droplets has significant role to play. As soon as the droplets come in contact with hot gas, the evaporation of solvent molecules commences creating a capillary pool among the dispersed particles. The attractive capillary force serves as the necessary external drive to overcome the potential barrier, and subsequently, the particles get interlocked into a deep potential well. Thus, the drying of the colloidal droplets inside the spray drying chamber induces self-assembly of nanoparticles resulting into nano-structured micro-granules. At larger distances, the energy profile goes through a maximum, and subsequently, passes through a barrier and then a shallow minimum, which is referred to as the secondary minimum. It should be noted that during the evaporation of solvent from a tiny colloidal droplet, the distance between particles starts to decrease due to capillary force. If the capillary forces are strong enough, attractive force can overcome the barrier leading to interlocking of particle into a deep potential well. This suggests that such induced assembly during the evaporation of solvent from tiny colloidal droplets can be a great way to realize nano-structured granules constituting interlocked nanostructures.

Let us discuss about physicochemical parameters that influence the drying rate of a droplet. The first factor which affects the drying is the phase change from liquid to vapour, i.e. the rate at which molecules escape the liquid–air interface [14]. The

second factor is the transport of the vapour molecules away from the droplet surface in the surrounding air. This transport can be purely diffusive [15], or a combination of diffusive and convective transport. The third rate-limiting factor is the evaporative cooling and heat transfer to the liquid–air interface [16]. The drying of droplets under atmospheric condition is mostly governed by the diffusive transport of vapour. The shrinkage of the isolated spherical droplet during drying under atmospheric condition is governed by the following equation [17]:

$$R_0^2 - R^2(t) = \frac{2D_v m_v}{\rho k T} (P_s - P_\infty)t \quad (11.2)$$

where ‘ R_0 ’, ‘ $R(t)$ ’ is radius of droplet at $t = 0$ and t , respectively; ‘ D_v ’ and ‘ m_v ’ are diffusion coefficient and molecular mass of water vapour, respectively. ‘ ρ ’ is the mass density of water. ‘ P_s ’ is the saturation vapour pressure at the surface of the droplet, and ‘ P_∞ ’ is the vapour pressure at a distance very far from the droplet, ‘ k ’ is Boltzmann constant and ‘ T ’ is absolute temperature. The shrinkage rate of the droplet deviates from Eq. (11.2) when it contains disperse or dissolved phase. Equation (11.2) suggests that typical drying time of an isolated water droplet of micrometer size in vacuum ($P_\infty \sim 0$) is extremely small and is typically less than millisecond order. However, in reality in a spray dryer, there are plenty of droplets instead of a single droplet. These droplets make ‘ P_∞ ’ significant, and drying time is relatively more than that for a drying of a single droplet in vacuum.

It is important to discuss how the self-assembly of colloids takes place during drying of contact-free spray droplets. Here, only two dominant processes are considered that play crucial role in the assembly of colloids during drying. The first process is shrinkage of droplet which depends on rate of drying that depends on the temperature, aspiration rate, etc. The second process is the diffusion of colloids inside the droplet. These two phenomena are competing in nature as far as the assembly nature of the particles is concerned. The shrinkage of the droplet results into the accumulation of the colloids near droplet surface, whereas diffusion of colloids makes the concentration of the colloids uniform throughout droplet. A dimensionless parameter, known as Peclet number (P_e) is defined as follows:

$$P_e = \frac{\tau_{\text{mix}}}{\tau_{\text{dry}}} = \frac{R^2}{D\tau_{\text{dry}}} \quad (11.3)$$

where ‘ τ_{dry} ’ is the drying time of the droplet and ‘ τ_{mix} ’ is the mixing time, i.e. diffusion time of the colloidal particles from the droplet surface to its centre. ‘ R ’ is the radius of the droplet. ‘ D ’ is the diffusion coefficient of colloidal particles (radius r) in the droplet. The diffusion coefficient for Newtonian fluids can be expressed using Einstein-Stokes, as $D = \frac{kT}{6\pi\eta r}$. The case when $P_e \ll 1$ implies that the diffusion of colloids is faster than the shrinkage rate of droplet. In this case, concentration of the colloids remains uniform across the droplet, and the droplet shrinks isotropically throughout the drying process resulting into spherical granule [10, 18, 19]. This

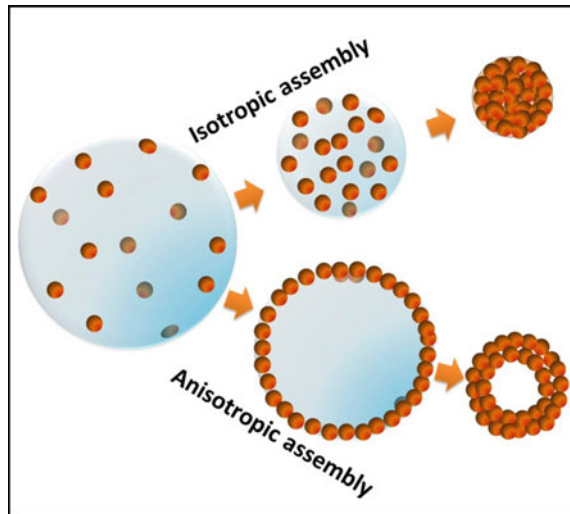
scenario is considered as slow drying, and no buckling of the drying colloidal droplet is expected in contrast to the fast-drying regime. Under the slow-drying regime using mass balance during drying, one can derive a relation between the droplet radius and volume fraction of colloids.

$$R^3(t)\phi(t) = R_0^3\phi_0 \quad (11.4)$$

where ' R_0 ' and ' ϕ_0 ' are the radius of the droplet and volume fraction of the colloids before drying, respectively. ' $R(t)$ ' and ' $\phi(t)$ ' are instantaneous radius and volume fraction of colloids at time ' t ', respectively.

Peclet number $P_e \gg 1$ implies that diffusion of colloids is slower compared to the shrinkage rate of the droplet leading to preferential accumulation of colloids at air–water interface of the droplet. A visco-elastic shell of the colloids is formed during drying followed by a visco-elastic to elastic transition that takes place due to the interlocking of the colloidal particles. The mechanical response of the elastic shell, under further compression of the droplet, may cause buckling of the shell resulting into complex morphology of the granules [20, 21], such as doughnut-shaped granules. The buckling of the shell indeed depends on its elastic properties and relative thickness [21]. Such drying scenario for $P_e \gg 1$ is regarded as fast-drying regime. A scenario of slow and fast-drying processes is shown schematically in Fig. 11.4. It should be noted that if the initial droplets are polydisperse in nature, the Eq. (11.4) suggests that an isotropic drying will make the size distribution of the granules much narrower (Fig. 11.5) compared to the size distribution of the initial droplets. Further, the size distribution of the granules obtained by anisotropic drying will be broader compared to that obtained by isotropic drying (Fig. 11.5). So, accurate measurements of droplet size distribution and the granular size distribution (either

Fig. 11.4 Schematic representation of isotropic assembly at slow drying and anisotropic assembly at fast-drying scenario



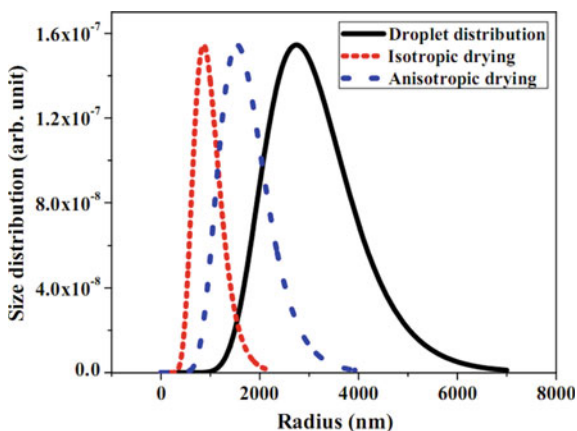


Fig. 11.5 Schematic representation of initial droplet size distribution and final granular size distribution under isotropic and anisotropic assembly scenario

by electron microscopy or by scattering techniques) can hint, in principle, about the nature of drying, isotropic or anisotropic. The jamming of colloids gives rise to the formation of mesopores owing to the presence of interstices between the jammed colloids. The pore size and specific surface area depend on the size of colloids and nature of jamming [22]. The spray drying technique can also be used to obtain pores with tunable size and porosity. The soft template such as polymer, surfactant and bacteria with hard colloids, such as silica, can be used to obtain the composite granules. The removal of the softer component results into templated pores [23] in the self-assembled granules. Figure 11.6 illustrates the template mechanism during drying of droplet under slow-drying regime.

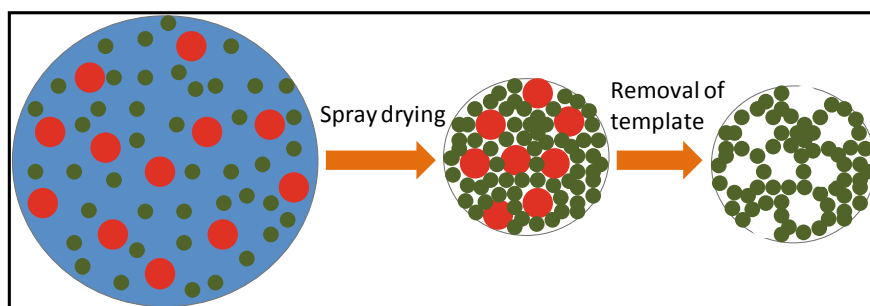


Fig. 11.6 Schematic representation of template mechanism during spray drying

11.4 Characterization Techniques

Often use of multiple characterization techniques become indispensable to gain insight into hierarchical structure of the assembled granules. The direct techniques like electron microscopy provide topological information of granules such as its shape and size. Electron microscopy, in particular, scanning electron microscopy (SEM) is the most suitable tool for investigating granules of micron size and below. However, internal structure of the granules such as packing fraction of colloids and nature of jamming cannot be probed using SEM. Further, standard transmission electron microscopy (TEM) is also not a very effective tool for getting internal structure of the granules due to limited penetration of electrons through the micron size granules. Moreover, real-time measurements during assembly of colloids are not feasible using microscopy techniques. Small-angle scattering (SAS) [24–26] using neutron and X-rays is an ideal technique to probe self-assembled granules having hierarchical structure [27]. Basic principle of microscopy and small-angle scattering technique is compared in Fig. 11.7. Microscopy techniques give information about object in real space whereas the scattering experiment provides information in reciprocal space. The microscopy and SAS methods are complementary techniques to probe the hierarchical nanostructures. We will describe SAS technique in a more detailed manner.

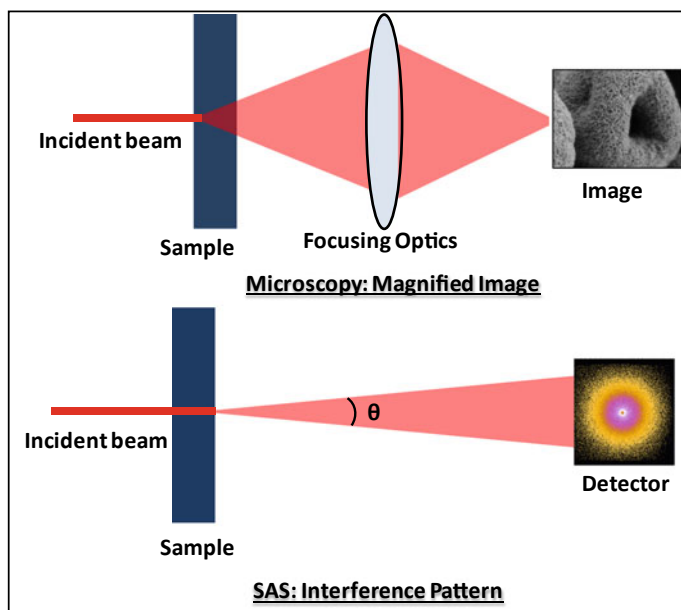


Fig. 11.7 Comparison of basic principle of the microscopy and small-angle scattering techniques

SAS provides structural information on inhomogeneities of mesoscopic dimension (1–1000 nm); structural features include size, shape, dimensionality and interparticle spatial correlation. The radiations such as X-rays, neutron and electrons interact with matter differently. Electrons being a charged particle interacts with matter strongly, hence, penetration of electron in the matter is less. This makes electrons as a local probe of the matter. Neutron is a neutral particle and hence it interacts with matter weakly. The penetration power of the neutron is quite high that makes it bulk probe of the matter. The X-ray interacts with matter via electromagnetic forces, the penetration power of X-rays falls in between that of electron and neutron.

X-rays and neutrons can be used as probe for SAS depending on the contrast it offers between the object and matrix where the objects are embedded. The strength of scattering of X-rays and neutron by an atom is quantified as scattering length. For X-ray, scattering length for each element scatters proportionally to its number of electrons. This indicates that scattering profile measured in an X-ray experiment will be primarily defined by the scattering from heavy Z elements. Neutron scattering lengths are determined by the quantum mechanics of the neutron–nucleus interaction and they vary irregularly across the periodic table. The basic differences between X-rays and neutrons as a probe for material are tabulated in Table 11.1.

In a SAS experiment, neutron/X-ray is incident on the sample with wave vector ' \mathbf{K}_i ' and is scattered into the state with wave vector ' \mathbf{K}_f '. The intensity of scattered neutron/X-rays is thus measured as a function of momentum transfer (see Fig. 11.8): $\mathbf{q} = (\mathbf{K}_f - \mathbf{K}_i)$ where \mathbf{q} is known as the wave vector transfer. The magnitude of a wave vector is defined as its wave number: $|\mathbf{K}| = K = 2\pi/\lambda$, where λ is the wavelength. For elastic scattering process $|\mathbf{K}_f| = |\mathbf{K}_i| = K$ and the magnitude of wave vector transfer ' \mathbf{q} ' is given by $|\mathbf{q}| = q = \frac{4\pi}{\lambda} \sin\theta$, where ' 2θ ' is the scattering angle. The detailed theory of small-angle scattering and its analysis procedure can be found in literatures [24–26, 28]. The scattering intensity from a two-phase particulate system can be expressed as,

Table 11.1 Comparison of the various scattering parameters for Neutron and X-ray

Parameter	Neutron	X-ray
Intensity	Low	High
Hydrogen-sensitivity	High	None
Isotope-sensitivity	Strong	None
Heavy elements	Low	High
Spin-sensitivity	Strong	Average
Penetration depth	High	Low
Sample size/amount	Large	Small
Measurement time	Long	Short
Interaction	Nuclear (No systematic variation with Z), Magnetic	Electron (varies as Z^2)
Radiation damage	Negligible	High

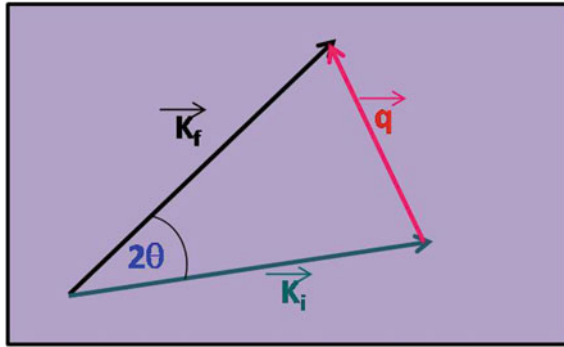


Fig. 11.8 The scattering law for elastic scattering scenario

$$I(q) = NV_p^2(\Delta\rho)^2P(q)S(q) \tag{11.5}$$

where ‘ N ’ is the number density of scattering objects, ‘ V_p ’ is the particle volume and ‘ $(\Delta\rho)^2$ ’ is the contrast factor. The term ‘ $P(q)$ ’ is a dimensionless function known as form factor that describes scattering from a single particle and is dependent on both its shape and size. Analytical expressions for ‘ $P(q)$ ’ have been available in the literatures for most common shapes [25, 28]. Form factors of sphere of radius R can be written as $P(q, R) = 9 \left[\frac{\sin(qR) - (qR)\cos(qR)}{(qR)^3} \right]^2$. The form factors of sphere of radius 20 nm, disk of radius 20 nm and cylinder of cross-section radius 20 nm and length 500 nm are shown in Fig. 11.9a. It is clear from this figure that functionality of the scattering profile significantly depends on the shape of scattering object. The slope of the scattering profile (log–log scale), in a particular q -range, shows $\sim q^{-1}$ and q^{-2} scattering behaviour for cylindrical and disk-shaped objects, respectively.

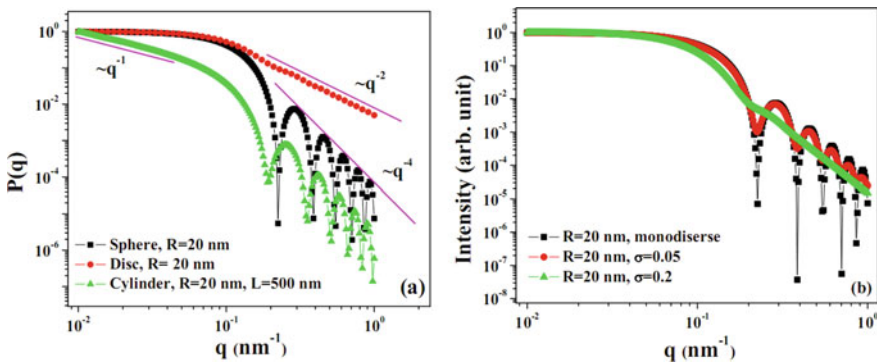


Fig. 11.9 **a** Form factor corresponding to different shapes of the particles is shown. Radius of sphere $R = 20$ nm, disc radius $R = 20$ nm, length L and radius of cylinder are 20 nm and 500 nm, respectively. **b** Effect of polydispersity on the scattering profiles

The scattering from spherical objects shows $\sim q^{-4}$ Porod scattering behaviour at high- q . The scattering intensity for a dilute system, where the distance between particles is much higher than their sizes, depends only on the form factor. In such a situation, interference between scattering from different particles may be neglected, and the measured signal carries information on the shape and size of individual particle. As the concentration of particle increases, the interference effects between scattering particles in the sample becomes important and is described by another dimensionless function ' $S(q)$ ' that is called structure factor. ' $S(q)$ ' depends on the spatial arrangements of the scattering objects, i.e. the correlations in their position and interactions. Its formula is given by:

$$S(q) = 1 + 4N\pi \int \left[(g(r) - 1)r^2 \frac{\sin(qr)}{qr} dr \right] \quad (11.6)$$

where ' $g(r)$ ' is the particle pair distribution function which describes the spatial distribution of the particles as a function of the average separation distance, ' r '. Analytical expressions for the structure factors have been derived for hard sphere interaction [29], sticky hard spheres between particles [28, 30, 31]. Similarly, for charged particle, structure factor has been derived using screen Coulomb interaction. Please note that Eq. 11.5 is valid for monodisperse particles only. For an ensemble of polydisperse particles, under local monodisperse approximation [32], the expression of the scattering intensity can be written as,

$$I(q) = N(\Delta\rho)^2 \int V_p^2(R)P(q, R)D(R)S(q, R)dR \quad (11.7)$$

where, ' $D(R)$ ' is the size distribution of the particles.

The structure factor $S(q) \sim 1$ for dilute ensemble of polydisperse particles and the Eq. 11.7, in this case, can be written as:

$$I(q) = N(\Delta\rho)^2 \int V_p^2(R)P(q, R)D(R)dR \quad (11.8)$$

The effect of the polydispersity on the scattering profiles from an ensemble of spheres possessing lognormal size distribution

$$D(R) = \frac{1}{\sqrt{2\pi\sigma^2}r^2} \exp\left(\frac{-(\ln(R/\mu))^2}{2\sigma^2}\right) \quad (11.9)$$

is shown in Fig. 11.3b. μ is the median of the size distribution and σ is called polydispersity index that varies between 0 and 1. It is evident that sharp oscillations in the scattering profiles get smeared as the polydispersity index increases (Fig. 11.9b).

Figure 11.10a depicts both the form factor and structure factor as a function of q ; the intensity obtained by multiplication of these two factors using Eq. 11.5 is also

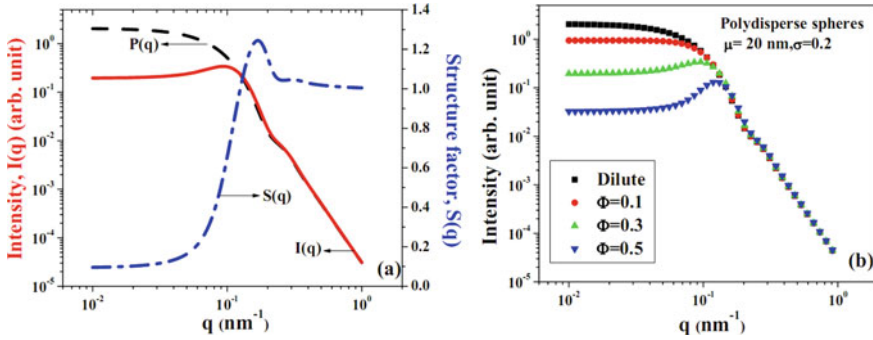


Fig. 11.10 **a** Scattering intensity is shown as multiplication of form factor and structure factor. **b** Effect of concentration of particle on the scattering profiles is depicted. Structure factor corresponding to the hard sphere interaction [29] under local monodisperse approximation [32] is used for modelling the data

shown. Polydisperse sphere with $\mu = 20$ nm and $\sigma = 0.2$ is assumed for calculation of ‘ $P(q)$ ’. Hard sphere type interparticle interaction was considered for the simulation of the structure factor ‘ $S(q)$ ’. It is observed from Fig. 11.5a that low- q intensity is governed by structure factor whereas the high- q scattering is dominated by the form factor. Figure 11.10b shows the scattering profiles as a function of volume fraction of the particle. The scattering intensity at low- q decreases with increasing volume fraction, a correlation peak starts building up at higher volume fraction $\phi \sim 0.3$ and it becomes sharp and shifts to high- q as ϕ increases to 0.5. The average distance between particles ‘ d_p ’ in a concentrated system is approximately related to peak position q_{peak} as $d_p \sim 2\pi/q_{\text{peak}}$.

In general, the granules obtained by spray drying process possess hierarchical structure of the jammed colloid. SAS profile in a wide- q -range can provide information about such the granule and the jamming nature of colloids. It should be mentioned that accessing scattering data over such a wide- q -range always remains a challenge due to limited q window of a particular instrument. In general, usage of conventional pin-hole small-angle scattering instrument [33] as well as double crystal-based ultra-small-angle scattering instrument [34] becomes necessary for investigating such granules. A simplistic model has been shown below to describe the scattering intensity from such assembled granule [35, 36]:

$$I(q) = C_g I_g(q) + C_{jc} I_{jc}(q) \tag{11.10}$$

where ‘ $I_g(q)$ ’ is the scattering contribution due to overall assembled granules and ‘ $I_{jc}(q)$ ’ is scattering contribution due to jammed colloids. ‘ C_g ’ and ‘ C_{jc} ’ are scale factor for granule and jammed colloid scattering contributions, respectively. It is to be noted that above equation is valid only if size of granules is quite large (order of the magnitude) compared to the size of individual colloidal particles.

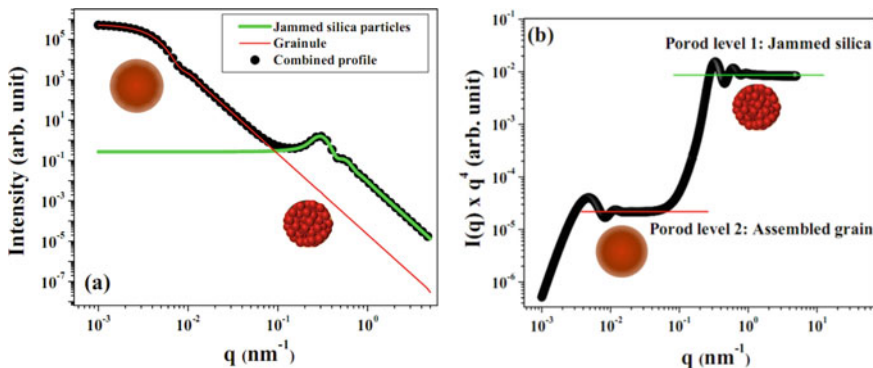


Fig. 11.11 Simulated small-angle scattering profile for assembled silica granules obtained by spray drying **a** $I(q)$ versus q . **b** $I(q) \times q^4$ versus q , i.e. in Porod representation

The first term in Eq. 11.10 gives information regarding the shape and size of the assembled granules, whereas second term in Eq. 11.10 provides information about the individual colloids such as its shape, size and nature of jamming. An ensemble of polydisperse spherical granules with $\mu = 500$ nm and $\sigma = 0.2$ has been taken as model for granule scattering $I_g(q)$. Randomly jammed colloids interacting via hard sphere interaction with a volume fraction $\phi \sim 0.54$ is taken as model to express $I_{jc}(q)$. Figure 11.11a shows simulated scattering profiles $I_g(q)$ and $I_{jc}(q)$ corresponding to scattering from over all granule and correlated colloids, respectively. The combined scattering intensity, i.e. sum of these scattering contributions is also shown in Fig. 11.11a in double logarithmic scale. The two-level structure is evident in Fig. 11.11b where data is plotted in Porod representation, i.e. $I(q) \times q^4$ versus q . Two constant levels in Porod plot indicate the presence of two-level structure in well-separated length scales. The Porod level at high- q is due to the scattering from individual colloid, whereas the Porod level at low- q is attributed to the scattering from overall granules.

11.5 A Few Illustrative Examples

11.5.1 Nano-structured Silica Micro-granules with Spherical and Doughnut Morphology

Silica micro-spheres as inorganic supports have become increasingly important for a variety of applications, including isolation of nucleic acids, cell separation and immuno- and DNA-based assays. They offer combined advantage of a broad platform and unique properties of a silica substrate. Silica micro-granules can be synthesized by spray drying technique with silica nano-suspension as starting material. The shape

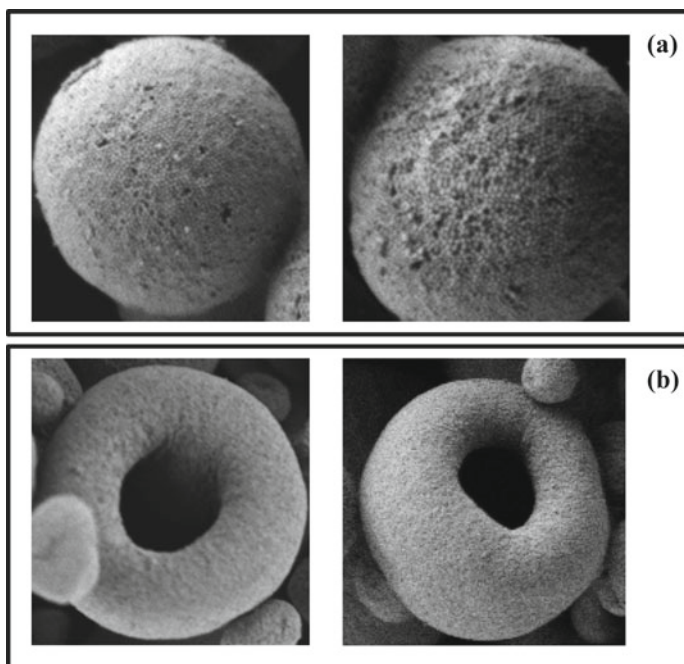


Fig. 11.12 FESEM micrographs showing: **a** spherical and **b** doughnut-shaped nano-structured silica granules. Reproduced with permission from Ref. No. 40 (Adapted with permission from (Biswas et al. Langmuir 2016. **32**(10); p. 2464–2473) Copyright (2016) American Chemical Society)

of the granules can be tuned by controlling the physicochemical conditions during spray drying [37]. Figure 11.12a, b shows spherical and doughnut-shaped granules, respectively. The formation of doughnut-shaped granules may be explained due to buckling of the shell formed during the rapid anisotropic drying as mentioned earlier [13, 20, 37–39].

It may be recalled from the earlier section that the Peclet number (P_e), signifying the nature of assembly, is given by $P_e = \frac{\tau_{\text{mix}}}{\tau_{\text{dry}}} = \frac{R^2}{D\tau_{\text{dry}}}$, where the diffusion coefficient of the nanoparticles in the droplet is ' D '. An increase in drying rate decreases ' τ_{dry} '. This in turn increases ' P_e '. It has been observed experimentally that gradual increase in drying rate results in increase in hollowness and subsequent buckling into doughnut shape [40]. The quantitative information on silica-silica correlation in the granules may be obtained from detail analysis of small-angle scattering profiles (Fig. 11.13). The correlation peak $\sim 0.2 \text{ nm}^{-1}$ in SAS profiles appears due to interparticle interference among the jammed silica particles in the granules.

These nanoporous silica granules have been found potential sorbents for cationic dyes such as methylene blue [41]. It needs to be mentioned that after sorption, the granules settle faster (Fig. 11.14), and thus allows easy decantation of the solvent in contrast to the situation with bare nanoparticles. It has been found [22, 42] that incorporation of such granules in ultra-filtration polysulphone membrane enhances

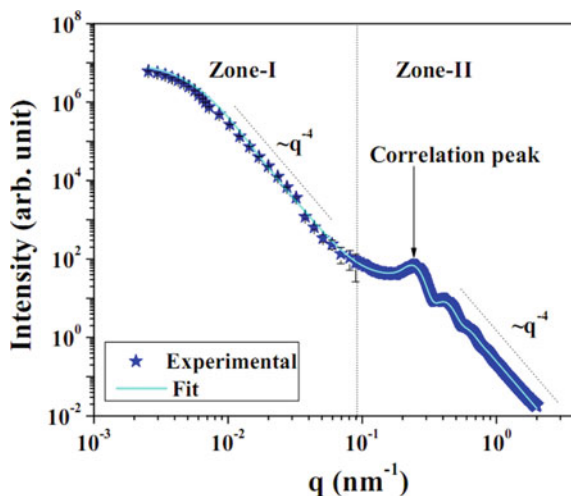


Fig. 11.13 Combined SAXS (Zone-I) and medium resolution SANS (Zone-II) data for nano-structured silica micro-granules. Reproduced with permission from Ref. No. 40 (Adapted with permission from (Langmuir 2016, **32**(10): p. 2464–2473) Copyright (2016) American Chemical Society)

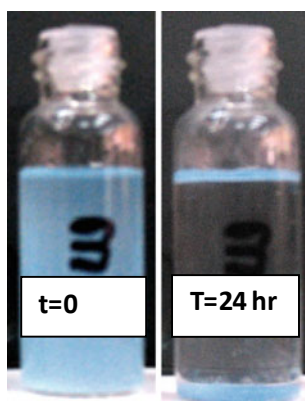


Fig. 11.14 The sorption of methylene blue dye by the granules from aqueous solution. The micro-granules, being heavier than bare nanoparticles, settle fast allowing easy decantation of the solvent after sorption. [41] Reproduced with permission from Ref. (Adapted with permission from Colloids and Surfaces A: Physicochem. Eng. Aspects 520 (2017) 279–288)

the pure water permeability quite significantly without affecting its rejection characteristics. This is probably because of the fact that the incorporated granules can offer suitable porous channels across membrane surface which were otherwise not accessible because of the tapering of the pore channels in casted membranes.

11.5.2 Macro/Meso Porous Silica Micro-spheres Using Template Mechanism

It is discussed earlier that spray drying is an effective technique to achieve macro/meso porous materials using template mechanism. Herein, an example of fabrication of macroporous silica granules has been shown which was obtained using *E. coli* bacteria as a template. *E. coli* are one of the primary bacterial contaminations in drinking water in most of the underdeveloped/developing countries including India. A unique approach is adopted to obtain silica-based macroporous micrometric granules for potential application of filtration of *E. coli* bacteria from drinking water using spray drying technique.

Initial silica dispersion (Visa Chemicals, Mumbai, India) was diluted in pure water (Milli-Q, Millipore). 2wt % silica dispersion and varying *E. coli* (0, 2, 4 and 6% in weight), soft component, were taken for spray drying. The inlet temperature was kept at 170 °C and the aspiration rate was kept at $\sim 47\text{m}^3/\text{h}$. The dried powders were collected from the cyclone separators. Removal of the imprinted materials was done by incineration in muffle furnace at 300 °C for 10 h. The powders, with 0, 2, 4 and 6% of *E. coli*, are designated as S0, S2, S4 and S6, respectively.

The SEM micrographs of samples S0–S6 are shown in Fig. 11.15a–c. It is evident that spray drying of the only silica colloids results into doughnut type granules as explained in previous section. The imprinting of *E. coli* in silica granule is also evident from the figure. The macroporosity of the spray-dried granules increases with increasing concentration of the *E. coli* in the initial dispersion used for spray drying. Interestingly, deformation of the assembled granules is increased at higher concentration of *E. coli*. It has been observed from Zeta potential measurements [9] that both silica and *E. coli* possess negative charge, and thus forms a repulsive system. During drying process of mixed colloids, the bigger size component diffusion is slow, and hence it remains primarily on the surface of the droplet during drying. Thus, the shell formed during drying consists of silica as well as *E. coli* leading to inhomogeneous shell. Subsequent compression of the droplet leads to the multi-faceted doughnut-shaped granule through buckling of elastic shell. The buckling gets enhanced with increase in softer component on the shell [39].

The arrest of buckling of the droplet containing mixed colloids requires prevention of shell formation or increase in elastic strength of the formed shell. In order to tune this aspect, *E. coli* cells were treated to impart a cationic charge on the cell surface using polyethylenimine (PEI) (Average MW $\sim 7.5 \times 10^5$). *E. coli* cells were treated with PEI 0.2, 1 and 2%, respectively. The Zeta potential measurements show that charge on *E. coli* becomes positive due to PEI coating and magnitude of charge increases with increasing coating thickness [9]. The spray drying of the 2wt% silica and PEI-treated *E. coli* have been performed with identical drying parameters used previously. The dried granules obtained for 0.2, 1.0 and 2.0 wt% PEI-treated *E. coli* have been designated as ST1, ST2 and ST3, respectively. Figure 11.15d–f show the micrographs of spray-dried granules obtained for

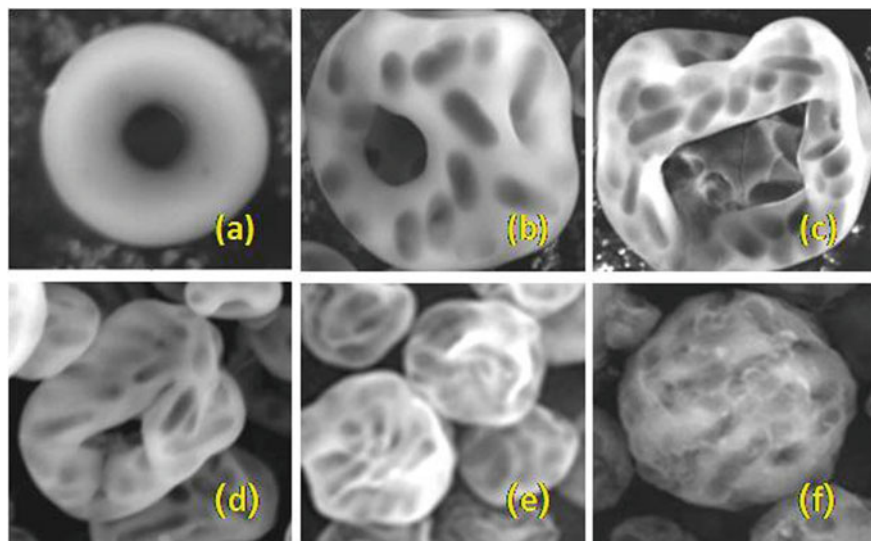


Fig. 11.15 SEM micrographs of **a** 2wt% silica, **b** 2wt% silica + 2wt% *E. coli*, **c** 2wt% silica + 6wt% *E. coli*. Reproduced with permission from Ref. No. 20 (From D. Sen et al., Buckling-driven morphological transformation of droplets of a mixed colloidal suspension during evaporation-induced self-assembly by spray drying. EPJ-E, 2010. 31(4): p. 393–402 with kind permission of The European Physical Journal (EPJ)) **d** 2wt% silica + 6wt% *E. coli* coated with 0.2% PEI, **e** 2wt% silica + 6wt% *E. coli* coated with 1.0% PEI and **f** 2wt% silica + 6wt% *E. coli* coated with 2.0% PEI. Reproduced with permission from Ref. No. 9 (Reproduced from Ref. 9 with permission from the Royal Society of Chemistry)

mixed colloids containing PEI-treated *E. coli*. It is evident from the figure that deformation of the granules significantly reduces with increasing PEI coating. The silica nanoparticles coat the surface modified *E. coli* bacteria due to the attractive force between them. Thus, the formed shell, exposed to the air-water interface, primarily contains silica coated reinforced *E. coli* and that results in its improved elastic properties. The increase in the elastic strength of the shell causes arrest of buckling of drying droplet resulting in spherical granules. A schematic of the assembly mechanism is shown in Fig. 11.16.

In order to get the quantitative information about the macroporous assembled granules, SANS measurements have been carried out in a wide- q -range (Fig. 11.17). The data were analysed using three length scale model. First contribution originates from the jammed silica in the granules, while the second contribution arises due to scattering from the *E. coli* templated pores. The third contribution is due to the scattering from the overall granular shape. Table 11.2 shows the important fitting parameters as obtained from analysis.

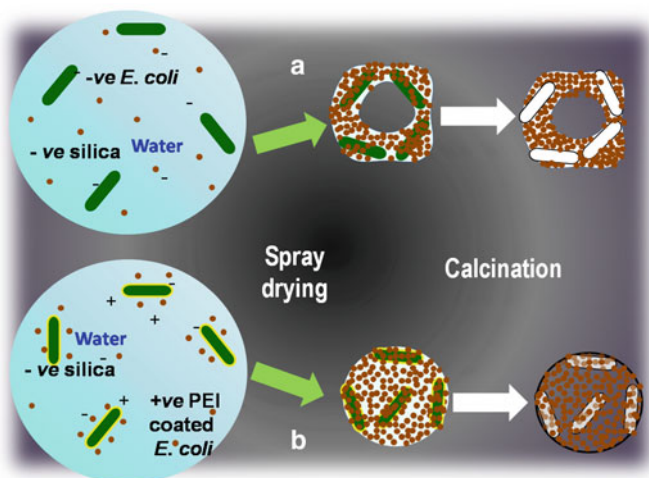
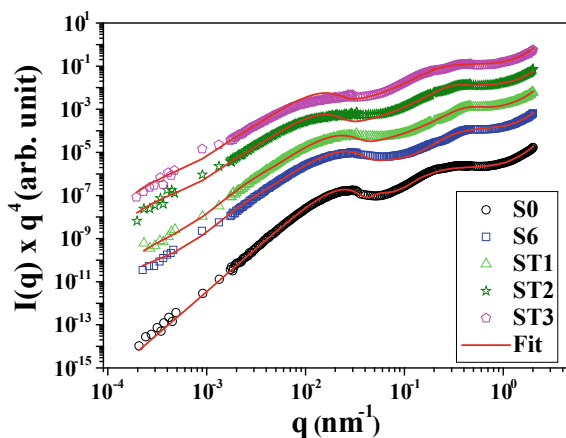


Fig. 11.16 Schematic representation of the assembly process of silica and E. coli. **a** Both silica and E. coli have negative surface charges and the system is repulsive. The assembled grains are deformed. **b** Silica is negative as in earlier case, but the E. coli surface is coated with PEI to impart positive charge on the E. coli surface. The assembled grains are spherical in this case and no buckling has occurred. [9] Reproduced with permission from Ref. No. 9 (Reproduced from Ref. with permission from the Royal Society of Chemistry)

Fig. 11.17 SANS profiles (Porod representation) of the E. coli template macroporous granules over a wide- q -range ([9] Reproduced from Ref. with permission from the Royal Society of Chemistry)



11.5.3 $\text{TiO}_2/\text{SiO}_2$ Nano-composites Via Spray Drying of Mixed Colloids

Spray drying technique has unique advantage because of its ability to mix colloids of similar size uniformly during the drying process. An example of fabrication of $\text{TiO}_2/\text{SiO}_2$ composite micro-spheres has been discussed below. TiO_2 -based materials

Table 11.2 Structural parameters obtained from SANS analysis. [9] Reproduced with permission from Ref. No. 9 (Reproduced from Ref. with permission from the Royal Society of Chemistry)

Sample	Assembled granule size distribution		Templated cylindrical macro pore		
	Mean radius (R_{granule}) (nm)	$\frac{\Delta R_{\text{grain}}}{R_{\text{grain}}}$	Length (L_{pore}) (nm)	Average radius (R_{pore}) (nm)	$\frac{\Delta R_{\text{pore}}}{R_{\text{pore}}}$
S0	200	0.099	–	–	
S6	2394	0.658	2000	102	0.205
ST1	2266	0.533	2050	115	0.209
ST2	2266	0.533	2600	167	0.305
ST3	2159	0.531	2600	167	0.305

are quite important due to their photocatalytic properties [43]. It is known that TiO_2 has three allotropes, namely, Anatase, Brookite and Rutile [44]. It is well established that anatase phase of TiO_2 is a more efficient photocatalyst as compared to its other allotropes [45]. However, the thermodynamic stability depends on particle size [46]. For particle size below ~ 14 nm, anatase phase is more stable than rutile phase. If TiO_2 nano-crystals are heated, crystal growth leads to alteration of phase stabilities and, ultimately, conversion of anatase phase to rutile phase takes place. Such phase transformation of anatase to rutile is considered to be one of the drawbacks for photocatalytic applications. Moreover, photocatalytic application of the TiO_2 requires a good dispersion of TiO_2 nanoparticles, as its efficiency increases because of availability of more surface area for reaction. Here, spray drying technique has been used to fabricate a $\text{TiO}_2/\text{SiO}_2$ composite that is stable against the anatase to rutile phase transformation. The incorporation of TiO_2 nanoparticles in the silica matrix leads to higher active surface area for the catalytic reaction.

A stable dispersion of the TiO_2 and SiO_2 has been mixed in the weight ratio of 2:1 for spray drying. The atomization pressure for the droplet generation was kept at 2.0 kg/cm^2 and inlet temperature during drying was fixed at 170°C . Solution feed rate was kept as 2 ml/min and aspiration rate was fixed at $50 \text{ m}^3/\text{h}$. The spray drying has also been carried out on the individual dispersions of SiO_2 and TiO_2 . The average size of the silica and titania colloids was determined using SAXS measurements [24, 25]. The average size of silica colloid was found to be ~ 16 nm, whereas the TiO_2 colloids possess bimodal size distribution with average size of 6 and 17 nm [47]. Figure 11.18 shows the SEM micrographs of the composite micro-spheres in low and high magnification. Nice spherical-shaped granules of micrometer size is achieved which is similar to the morphology of the TiO_2 and SiO_2 granules [47]. The energy dispersive X-ray (EDX) analysis was also carried out on the composite sphere which confirms the formation of $\text{TiO}_2/\text{SiO}_2$ composite (Fig. 11.18c).

Combined SANS profiles of the SiO_2 , TiO_2 and $\text{TiO}_2/\text{SiO}_2$ micro-spheres have been depicted in Fig. 11.19a. Scattering profiles are also shown in Porod representation ($I(q)q^4$ versus q) as depicted in Fig. 11.19b. It is evident from the figure that the assembled granules possess hierarchical length scale structure, and existence of two

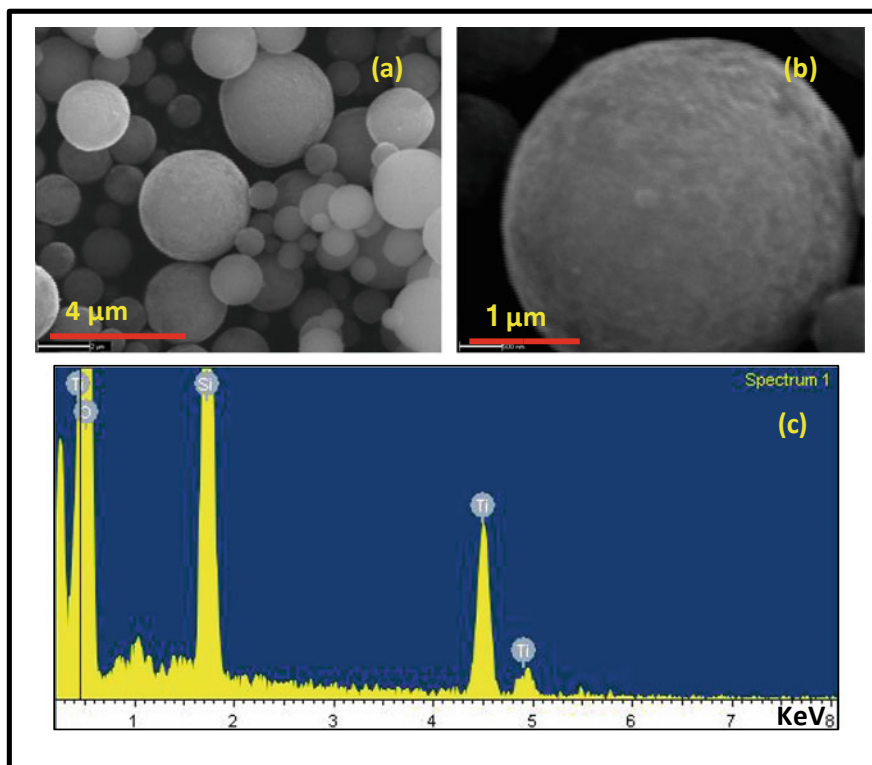


Fig. 11.18 $\text{TiO}_2/\text{SiO}_2$ micro-spheres: **a** in low and **b** high magnification (Adapted with permission from [47] Reproduced with permission from Ref. (Langmuir, 2012. 28(31): p. 11, 343–11, 353) Copyright (2012) American Chemical Society). The EDX spectrum of the composite is shown in (c)

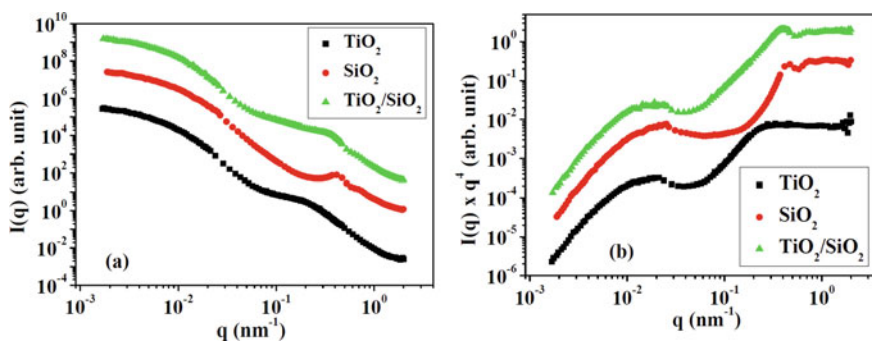
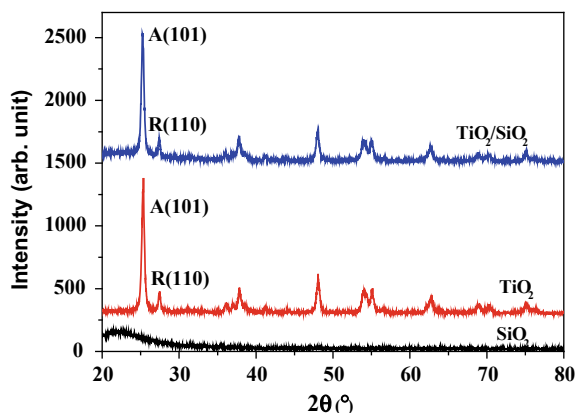


Fig. 11.19 SANS profiles of TiO_2 , SiO_2 and $\text{TiO}_2/\text{SiO}_2$ composite micro-sphere is shown in two representations. **a** $I(q)$ versus q and **b** $I(q) \times q^4$ versus q . [47] Reproduced with permission from Ref. (Adapted with permission from (Langmuir, 2012. 28(31): p. 11,343–11,353) Copyright (2012) American Chemical Society)

Fig. 11.20 XRD patterns of the TiO_2 , SiO_2 and the composite micro-spheres. [47] Reproduced with permission from Ref. (Reprinted with permission from (Langmuir, 2012. 28(31): p. 11, 343–11, 353) Copyright (2012) American Chemical Society)



Porod levels is evident. The SANS profile of silica micro-spheres shows a distinct correlation peak at $q \sim 0.45 \text{ nm}^{-1}$ corresponding to jammed silica nanoparticles, the oscillations in the scattering profiles is due to low polydispersity in the size of colloids. A relatively broader hump is observed in the SANS profile of TiO_2 micro-spheres because of relatively larger polydispersity in the size of TiO_2 colloids. SANS profile of the composite shows a silica correlation peak which is broader than that for SiO_2 granules. The X-ray diffraction (XRD) profiles have been recorded for all the samples and it is shown in Fig. 11.20. A broad hump is observed for the silica micro-sphere indicating the amorphous nature of the silica nanoparticles.

The TiO_2 micro-sphere shows the diffraction peaks indicating its crystalline nature. The phase identification reveals that both anatase and rutile phase exist in 85:15 weight ratio [47]. The position of (101) and (110) planes corresponding to anatase and rutile phase, respectively, is marked in the figure. The XRD measurements were performed on TiO_2 and composite that were heat-treated at different temperatures. The evolution of (101) and (110) planes of the anatase and rutile phase as a function of temperature is shown in Fig. 11.21. It is evident that anatase to rutile phase transformation occurs beyond $600 \text{ }^\circ\text{C}$ for TiO_2 micro-sphere. However, no phase transformation takes place in case of composite micro-sphere. This suggests that composite granules are thermally stable against anatase to rutile phase transformation. The growth of TiO_2 nano-crystal is hindered in the composite granules as it is surrounded by SiO_2 nanoparticles; this leads to arrest of phase transformation at higher annealing temperature. Thus, spray drying technique using binary colloidal systems is a one-step method to fabricate composite granules with improved properties. The structure and dispersion properties can be tuned by ratios of size of colloids and its concentration.

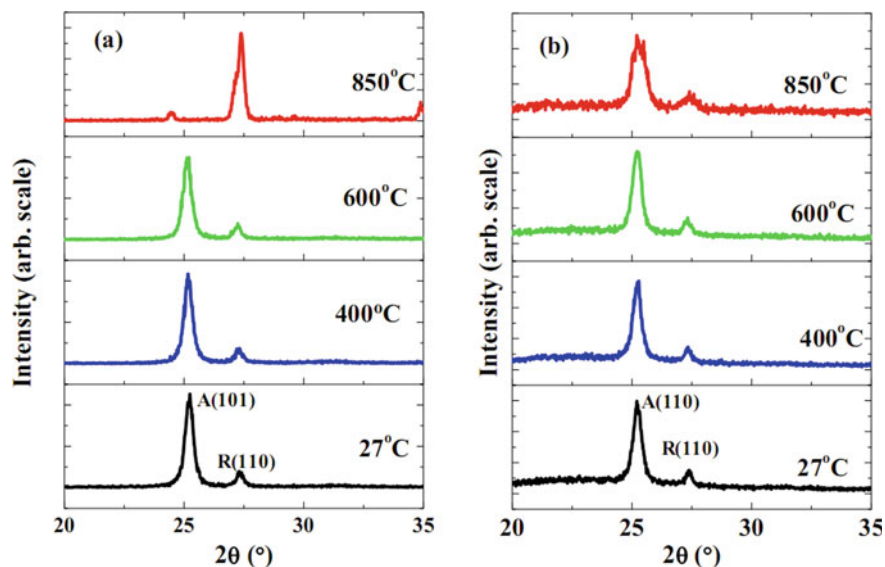


Fig. 11.21 XRD pattern of the TiO_2 and $\text{TiO}_2/\text{SiO}_2$ composite as a function of temperature. [47] Reproduced with permission from Ref. (Adapted with permission from (Langmuir, 2012, 28(31): p. 11,343–11,353) Copyright (2012) American Chemical Society)

11.5.4 Formation of Nano-composite Micro-spheres with Core–Shell Spatial Distribution

Spatial distribution of the building blocks during assembly may be controlled, and granules in the form of Janus [48] or Core–Shell [49] morphology can be synthesized in one-step process. Here, an example of core–shell micro-granules has been discussed, where contrasting interfacial interaction of two types of nanoparticles with solvent has been exploited during evaporation-induced self-assembly by spray drying. A mixed colloidal solutions of carbon black (from M/s. Hi-Tech Carbon of grade N-330) and silica (LUDOX® SM30 from M/s. Sigma Aldrich) nanoparticles are taken as feed to spray drying. The reason behind choosing carbon and silica is that they possess opposite polarity of water-affinity. Carbon being hydrophobic hates water molecules, whereas silica is hydrophilic in nature. The colloidal particles in mixed suspension remain dispersed in spatially random manner in water. However, after the colloidal suspension is sprayed inside the drying chamber, the fluid starts evaporating out of the droplet in radially outward direction. The movement of water molecules builds up a competition between hydrophilic and hydrophobic components. The water-loving component moves in radially outward direction along with water molecules, but water-repelling component tries to propel against the motion of water molecules and occupy water-depleted region. Thus, the contrasting interfacial interaction with solvent molecules creates a spatial distribution of hydrophilic and hydrophobic components in the drying droplet. The hydrophobic particles, i.e.

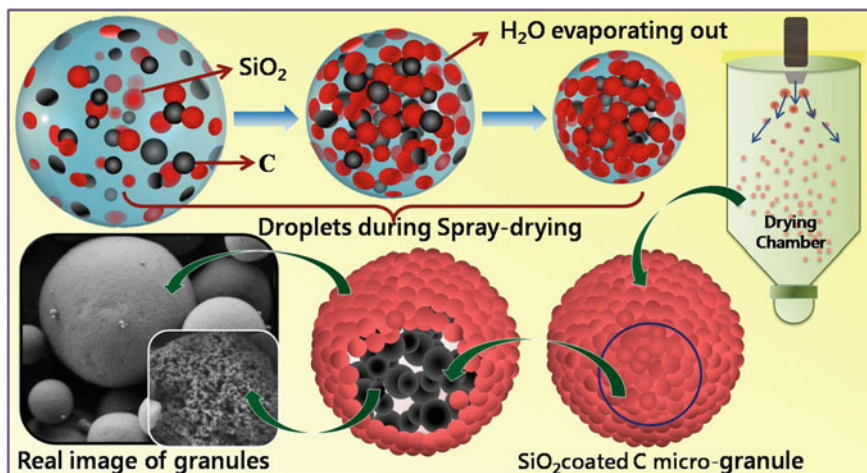


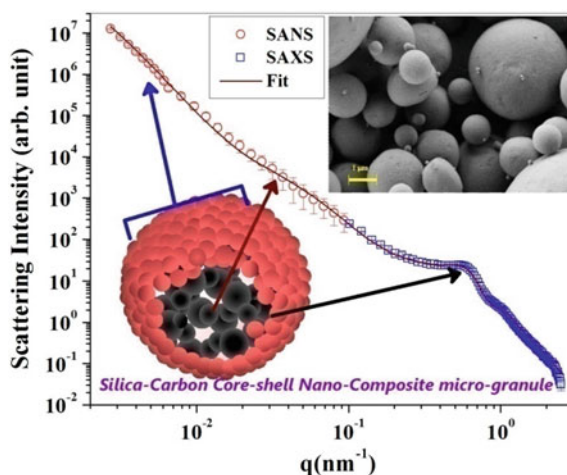
Fig. 11.22 Schematic representation of nano-composite core-shell micro-granules of carbon and silica. FESEM micrographs show silica-wrapped core-shell micro-granules and the carbon core after leaching. [42, 43] Reproduced with permission from Ref. (Reproduced from Ref. with permission from the Royal Society of Chemistry)

carbon nanoparticles assemble near the core, while hydrophilic particles, i.e. silica nanoparticles occupy the peripheral region of the droplet. In the course of drying, nano-structured carbon gets encapsulated by porous nano-structured shell of silica [42]. The schematic in Fig. 11.22 depicts how the contrasting interfacial interaction of nanoparticles with solvent has been utilized during evaporation-induced self-assembly to encapsulate nano-structured porous carbon core inside nano-structured porous silica shell.

SANS and SAXS measurements have been carried out to characterize the hierarchical mesoscopic structure of the spray-dried micro-granules. Combining SANS and SAXS (Fig. 11.23), a wide wave vector transfer range of three decades ($0.003\text{--}2.5\text{ nm}^{-1}$) has been accessed to map the positional correlation and particle form factor in mesoscopic length scale domain. In complementary to scattering investigations, field emission scanning electron microscopy (FESEM) has also been used to directly image the micro-granules in order to corroborate the results inferred from scattering.

The granules show unique features as far as application in water filtration is concerned. The hydrophilic shell of highly correlated nano-silica offers a wetting surface for convenient incorporation in polymeric ultra-filtration membrane. In addition to this, water transport occurs through the interstitial nano-pores towards the meso porous carbon core. It is to be noted that for decades, activated carbon is being used as water purification filter, because of its high specific surface area enabling adsorption of various organic compounds. Carbon is widely used in every household water filter for its high efficiency in maintaining the taste and odour of drinking water. In modern method of household drinking water purification, polymeric semi-permeable ultra-filtration membranes are also being exploited in separating colloidal

Fig. 11.23 Combined SANS and SAXS profile of the silica–carbon composite spray-dried granules. The inset shows the electron micrographs of the silica-wrapped spray-dried granules. [42, 43] Reproduced with permission from Ref. (Reproduced from Ref. with permission from the Royal Society of Chemistry)



and suspended matters from water [50, 51]. The carbon–silica nano-composite micro-granule, because of its core–shell morphology, is easy to incorporate into ultra-filtration membrane, and thus allow us to combine two separate filtration unit into a single one. The incorporation of these granules into a polymeric membrane has been accomplished and the performance is tested [42, 51]. Results reveal significant enhancement of water permeability (up to ~18%) through the micro-granules-incorporated membranes, and the rejection of PEO-100 K from water is almost 100% which has a huge impact as far as membrane separation characteristics are concerned. This is due to available interstitial pore channels and large specific surface of mesopores present in the micro-granules. The synthesized composite membrane, in comparison to standard polymeric membrane, can be utilized to gain the benefits of superior adsorption properties of mesoporous carbon combining with its own ultra-filtration separation characteristics with enhanced flux. Use of such silica–carbon composite membrane will make a household water filter substantially compact as the need for separate charcoal column, used in a standard filter, will become redundant.

11.6 Future Outlook

The representative studies discussed in this chapter show that the evaporation-induced assembly through spray drying technique is indeed a novel route to realize nano-structured micro-granules with interesting shape and pore structure. At this juncture, it is relevant to discuss the future prospects and associated challenges of this novel bottom-up technique. There are several aspects in this field which needs to be brought into closer scrutiny in order to understand this complex assembly procedure which crucially depends on several physicochemical parameters. Understanding the nature

of assembly of anisotropic colloids is highly desirable. Such assembly may ultimately result into a facile route in realizing porous granules with aligned ordered pore channels in the granules. Further, evaporative assembly of the anisotropic colloids can also be coupled with electric or magnetic field in realizing tunable architecture of granules. Apart from synthesis, the challenge remains in establishing an appropriate methodology in analysing small-angle scattering data from such granules with complex internal structure. Here, it is interesting to mention that random jamming of anisotropic particles is an interesting problem in general, and the established theory about the interparticle correlation in such concentrated system of anisotropic particles may be verified. Creation of Janus and core-shell granules by controlling the interparticle interaction during assembly still remains a challenge. Atomization, using three-fluid nozzle, of mixture of two colloids with contrasting hydrophilic and hydrophobic characteristics and proper tuning of interparticle interactions may result in such interesting morphology of the granules and thus needs attention. The inherent procedure of spray drying technique often involves hydrodynamic parameters apart from the thermodynamic parameters. Thus, it indeed remains a challenge to differentiate the individual role of these parameters in tuning the shape of the granules as well as the internal correlation of the nanoparticles. It is discernible from the above sections that such porous granules have several potentials for technological use including filtration and remediation depending on their shape and internal structure. Thus, challenge remains to optimize the synthesis parameters to tune the shape of the granules in addition to realizing extremely narrow distribution of their size. It is worthy to mention that in standard spray drying process, the coalescence of the droplets in the chamber at high feed rate remains an issue. Thus, experiments on levitated single drying colloidal droplets in an ultrasonic levitator may be useful in this regard while deciphering the role of various competitive physicochemical parameters. Further, it is worth mentioning that the effects of confinement on various chemical reaction equilibrium in nanoporous materials is an emerging field, and thus these porous granules may be used as host materials for such chemical reaction.

In short, evaporation-induced assembly of the colloidal particles in contact-free droplets can be realized through spray drying in order to obtain nano-structured micro-granules. The granular shape, internal correlation, porosity, etc., can be tuned by proper control of the governing parameters, including drying rate, viscosity, surface tension, size of colloids, interparticle interaction, etc. Such porous granules promise several technological applications.

References

1. Caruso F, Caruso RA, Möhwald H (1999) Production of hollow microspheres from nanostructured composite particles. *Chem Mater* 11(11):3309–3314
2. Martinez CJ, Hockey B, Montgomery CB, Semancik S (2005) Porous tin oxide nanostructured microspheres for sensor application. *Langmuir* 21(17):7937–7944
3. He Y (2005) Nanostructured CeO₂ microspheres synthesized by a novel surfactant-free emulsion. *Powder Technol* 155(1):1–4

4. He Y, Yu X, Zhao X (2007) Synthesis of hollow CuS nanostructured microspheres with novel surface morphologies. *Mater Lett* 61:3014–3016
5. Iskandar F, Mikrajuddin, Okuyama K (2001) In Situ production of spherical silica particles containing self-organized mesopores. *Nano Lett* 1:231–234
6. Martinez CJ, Hockey B, Montgomery CB, Semancik S (2006) Preparation of functional nanostructured particles by spray drying. *Adv Powder Technol* 17(6):587–611
7. Yunker PJ, Still T, Lohr MA, Yodh AG (2011) Suppression of the coffee-ring effect by shape-dependent capillary interactions. *Nature* 476:308–311
8. Sen D, Mazumder S, Melo JS, Khan A, Bhattacharya S, D'Souza SF (2009) Evaporation driven self-assembly of a colloidal dispersion during spray drying: volume fraction dependent morphological transition. *Langmuir* 25(12):6690–6695
9. Sen D, Melo JS, Bahadur J, Mazumder S, Bhattacharya S, D'Souza SF, Frielinghaus H, Goerigk G, Loidl R (2011) Arrest of morphological transformation during evaporation-induced self-assembly of mixed colloids in micrometric droplets by charge tuning. *Soft Matter* 7(11):5423–5429
10. Sen D, Khan A, Bahadur J, Mazumder S, Sapra BK (2010) Use of small-angle neutron scattering to investigate modifications of internal structure in self-assembled grains of nanoparticles synthesized by spray drying. *J Colloid Interface Sci* 347(1):25–30
11. Bahadur J, Sen D, Mazumder S, Santoro G, Yu S, Roth S, Melnichenko Y (2015) Colloidal nanoparticle interaction transition during solvent evaporation investigated by in-situ small-angle X-ray scattering. *Langmuir* 31(16):4612–4618
12. Sen D, Bahadur J, Mazumder S, Santoro G, Yu S, Roth SV (2014) Probing evaporation induced assembly across a drying colloidal droplet using in situ small-angle X-ray scattering at the synchrotron source. *Soft Matter* 10(10):1621–1627
13. Masters K (1991) *Spray drying handbook*, 5th edn. Longman Scientific and Technical, Harlow
14. Cazabat AM, Guena G (2010) Evaporation of macroscopic sessile droplets. *Soft Matter* 6(12):2591–2612
15. Popov YO (2005) Evaporative deposition patterns: spatial dimensions of the deposit. *Phys Rev E* 71(3): 036313
16. Dunn GJ, Wilson SK, Duffy BR, David S, Sefiane K (2009) The strong influence of substrate conductivity on droplet evaporation. *J Fluid Mech* 623:329–351
17. Frohn A, Roth N (2000) *Dynamics of droplets*. Springer, Berlin
18. Sen D, Spalla O, Tache O, Haltebourg P, Thill A (2007) Slow drying of a spray of nanoparticles dispersion. In situ SAXS investigation. *Langmuir* 23(8):4296–4302
19. Bahadur J, Sen D, Mazumder S, Paul B, Khan A, Ghosh G (2010) Evaporation-induced self assembly of nanoparticles in non-buckling regime: volume fraction dependent packing. *J Colloid Interface Sci* 351(2):357–364
20. Sen D, Melo JS, Bahadur J, Mazumder S, Bhattacharya S, Ghosh G, Dutta D, D'Souza SF (2010) Buckling-driven morphological transformation of droplets of a mixed colloidal suspension during evaporation-induced self-assembly by spray drying. *Eur Phys J E* 31(4):393–402
21. Tsapis N, Dufresne ER, Sinha SS, Riera CS, Hutchinson JW, Mahadevan L, Weitz DA (2005) Onset of buckling in drying droplets of colloidal suspensions. *Phys Rev Lett* 94(1):0183021–0183024
22. Sen D, Ghosh AK, Mazumder S, Bindal RC, Tewari PK (2014) Novel polysulfone-spray-dried silica composite membrane for water purification: Preparation, characterization and performance evaluation. *Sep Purif Technol* 123:79–86
23. Biswas P, Sen D, Mazumder S, Melo JS, Basak CB, Dasgupta K (2017) Porous nano-structured micro-granules from silica-milk bi-colloidal suspension: synthesis and characterization. *Colloids Surf B-Biointerfaces* 154:421–428
24. Glatter O, Kratky O (1982) *Small angle X-ray scattering*. Academic Press, New York
25. Guinier A, Fournet G, Walker BC, Yudowith LK (1955) *Small angle scattering of X-rays*. Wiley, New York
26. Windsor C (1988) An introduction to small-angle neutron scattering. *J Appl Crystallogr* 21(6):582–588

27. Boissiere C, Grosso D, Amenitsch H, Gibaud A, Coupé A, Baccile N, Sanchez C (2003) First in-situ SAXS studies of the mesostructuration of spherical silica and titania particles during spray-drying process. *Chem Commun* 2798–2799
28. Pedersen JS (1997) Analysis of small-angle scattering data from colloids and polymer solutions: modeling and least-squares fitting. *Adv Colloid Interface Sci* 70(Supplement C):171–210
29. Kinning DJ, Thomas EL (1984) Hard-sphere interactions between spherical domains in diblock copolymers. *Macromolecules* 17(9):1712–1718
30. Menon SVG, Manohar C, Rao KS (1991) A new interpretation of the sticky hard sphere model. *J Chem Phys* 95:9186–9190
31. Baxter RJ (1968) Percus-Yevick equation for hard spheres with surface adhesion. *J Chem Phys* 49:2770
32. Pedersen J (1994) Determination of size distribution from small-angle scattering data for systems with effective hard-sphere interactions. *J Appl Crystallogr* 27(4):595–608
33. Aswal VK, Goyal PS (2000) Small-angle neutron scattering diffractometer at Dhruva reactor. *Current Science*, 2000. 79(7).
34. Mazumder S, Sen D, Saravanan T, Vijayaraghavan PR (2001) A medium resolution double crystal based small-angle neutron scattering instrument at Trombay. *Curr Sci* 81(3):257–262
35. Thill A, Spalla O (2005) Influence of templating latex on spray dried nanocomposite powders studied by small angle scattering. *J Colloid Interface Sci* 291(2):477–488
36. Sen D, Spalla O, Belloni L, Charpentier T, Thill A (2006) Temperature effects on the composition and microstructure of spray-dried nanocomposite powders. *Langmuir* 22(8):3798–3806
37. Bahadur J, Sen D, Mazumder S, Paul B, Bhatt H, Singh SG (2012) Control of buckling in colloidal droplets during evaporation-induced assembly of nanoparticles. *Langmuir* 28(3):1914–1923
38. Sen D, Bahadur J, Mazumder S, Verma G, Hassan PA, Bhattacharya S, Vijai K, Doshi P (2012) Nanocomposite silica surfactant microcapsules by evaporation induced self assembly: tuning the morphological buckling by modifying viscosity and surface charge. *Soft Matter* 8(6):1955–1963
39. Bahadur J, Sen D, Mazumder S, Bhattacharya S, Frieinghaus H, Goerigk G (2011) Origin of buckling phenomenon during drying of micrometer-sized colloidal droplets. *Langmuir* 27(13):8404–8414
40. Biswas P, Sen D, Mazumder S, Basak CB, Doshi P (2016) Temperature mediated morphological transition during drying of spray colloidal droplets. *Langmuir* 32(10):2464–2473
41. Biswas P, Sen D, Mazumder S, Ramkumar J (2017) Porous microcapsules comprised interlocked nano-particles by evaporation-induced assembly: evaluation of dye sorption. *Colloids Surf A-Physicoche Eng Aspects* 520:279–288
42. Das A, Sen D, Mazumder S, Ghosh AK, Basak CB, Dasgupta K (2015) Formation of nanostructured core-shell micro-granules by evaporation induced assembly. *RSC Adv* 5:85052–85060
43. Shen X, Zhang J, Tian B, Anpo M (2012) Tartaric acid-assisted preparation and photocatalytic performance of titania nanoparticles with controllable phases of anatase and brookite. *J Mater Sci* 47(15):5743–5751
44. Reyes-Coronado D, Rodríguez-Gattorno G, Espinosa-Pesqueira ME, Cab C, Coss RD, Oskam G (2008) Phase-pure TiO₂ nanoparticles: anatase, brookite and rutile. *Nanotechnology* 19(14):145605
45. Scalfani A, Palmisano L, Schiavello M (1990) Influence of the preparation methods of titanium dioxide on the photocatalytic degradation of phenol in aqueous dispersion. *J Phys Chem* 94:829
46. Zhang H, Banfield JF (1998) Thermodynamic analysis of phase stability of nanocrystalline titania. *J Mater Chem* 8:2073
47. Bahadur J, Sen D, Mazumder S, Sastry PU, Paul B, Bhatt H, Singh SG (2012) One-step fabrication of thermally stable TiO₂/SiO₂ nanocomposite microspheres by evaporation-induced self-assembly. *Langmuir* 28(31):11343–11353
48. Gangwal S, Cayre OJ, Bazant MZ, Velev OD (2008) Induced-charge electrophoresis of metalloidielectric particles. *Phys Rev Lett* 100(5):058302

49. Klein MK, Saenger NR, Schuetter SP, Zumbusch A (2014) Shape-tunable core-shell microparticles. *Langmuir* 30(42):12457–12464
50. Upadhyayula VKK, Deng S, Mitchell MC, Smith GB (2009) Application of carbon nanotube technology for removal of contaminants in drinking water: a review. *Sci Total Environ* 408(1):1–13
51. Das A, Sen D, Mazumder S, Ghosh AK (2017) Nano-structured silica coated mesoporous carbon micro-granules for potential application in water filtration. *AIP Conf Proc* 1832(1):050094